ACS SyntheticBiology

pubs.acs.org/synthbio Research Article

Development of a Signal-integrating Reporter to Monitor Mitochondria–ER Contacts

Published as part of ACS Synthetic Biology special issue "Mammalian Cell Synthetic Biology".

Zheng Yang and David C. Chan*

Cite This: *ACS Synth. Biol.* 2024, 13, 2791–2803 Read Online

ACCESS | Metrics & More | Article Recommendations | Supporting Information

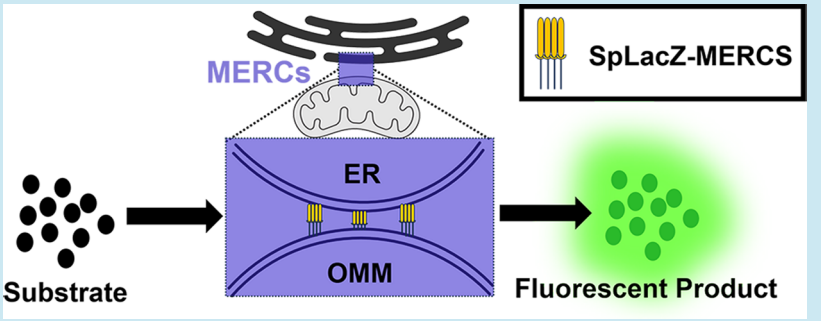

ABSTRACT: Mitochondria–endoplasmic reticulum contact sites (MERCS) serve as hotspots for important cellular processes, including calcium homeostasis, phospholipid homeostasis, mitochondria dynamics, and mitochondrial quality control. MERCS reporters based on complementation of green fluorescent proteins (GFP) fragments have been designed to visualize MERCS in real-time, but we find that they do not accurately respond to changes in MERCS content. Here, we utilize split LacZ complementing fragments to develop the first MERCS reporter system (termed SpLacZ-MERCS) that continuously integrates the MERCS information within a cell and generates a fluorescent output. Our system exhibits good organelle targeting, no artifactual tethering, and effective, dynamic tracking of the MERCS level in single cells. The SpLacZ-MERCS reporter was validated by drug treatments and genetic perturbations known to affect mitochondria–ER contacts. The signal-integrating nature of SpLacZ-MERCS may enable systematic identification of genes and drugs that regulate mitochondria–ER interactions. Our successful application of the split LacZ complementation strategy to study MERCS may be extended to study other forms of interorganellar crosstalk.

KEYWORDS: *mitochondria, endoplasmic reticulum, contact sites, organelle interactions*

INTRODUCTION

Mitochondria have major roles in promoting bioenergetic pathways, cell signaling, calcium homeostasis, and apoptosis.[1−3] In addition to true mitochondrial diseases, dysfunctional mitochondria have been linked to neurodegenerative diseases, including Parkinson's disease, amyotrophic lateral sclerosis, and Huntington's disease.[2−5] In recent years, interorganellar crosstalk has emerged as a factor influencing the cellular roles of mitochondria.[6−8] In particular, the endoplasmic reticulum (ER) closely interacts with mitochondria and modulates cellular physiology. Such interactions occur at mitochondria–ER contact sites (MERCS), which are close appositions of mitochondria and ER with a distance of ∼10−50 nm.[9] These contacts regulate a number of cellular processes, including calcium homeostasis, lipid homeostasis, mitochondrial dynamics, and mitochondrial quality control.[10−13] Although some mitochondria–ER tethers have been identified,[10,11,13−15] much remains to be understood about the regulation of MERCS dynamics.

Given the physiological importance of mitochondria–ER interactions, it is critical to develop new tools to understand their molecular basis and cellular functions. Several studies have described reporters designed to identify MERCS in single cells.[16,17] Most current reporter systems employ biomolecular fluorescence complementation (BiFC). Based on the splitting of fluorescent proteins into two complementary fragments, these assays target the fragments individually to mitochondria and ER. In locations where the two organelles are in close proximity, the two protein fragments are reconstituted into a functional protein whose chromophore matures. Split-green fluorescent proteins (GFP), split-red fluorescent protein (RFP), and split-Venus

Received: February 14, 2024
Revised: August 6, 2024
Accepted: August 6, 2024
Published: August 20, 2024

https://doi.org/10.1021/acssynbio.4c00098
ACS Synth. Biol. 2024, 13, 2791–2803

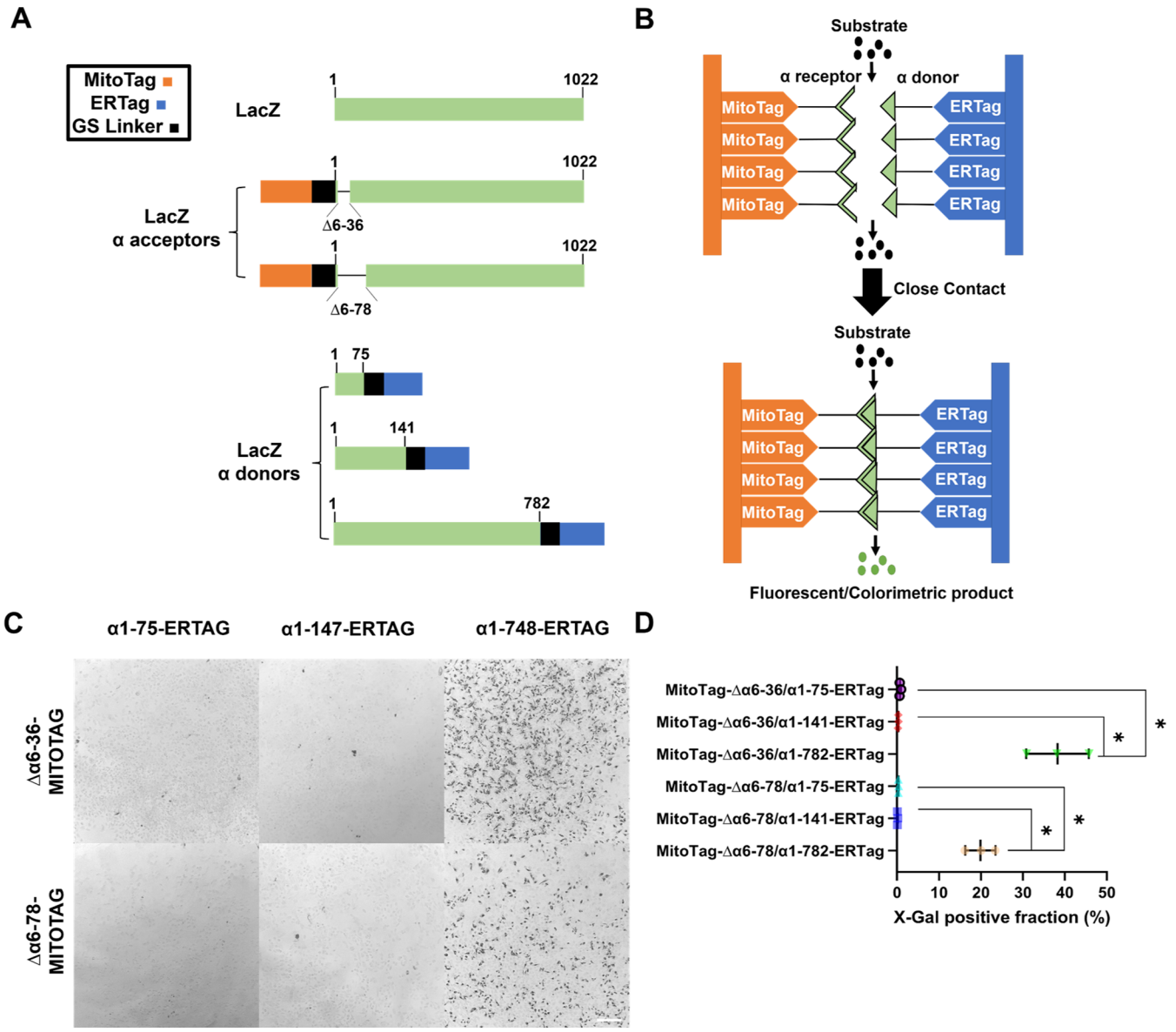

Figure 1. Constructs and concept of split LacZ-based mitochondria−ER contact site (MERCS) reporter. (A) Schematic of the two mitochondria-targeted LacZ α acceptors ($\Delta\alpha$6-36, $\Delta\alpha$6-78) and the three ER-targeted LacZ α donors (α1-75, α1-141, and α1-782). The top green rectangle indicates the full-length LacZ gene. MitoTag is derived from the N-terminal transmembrane sequence from Tomm70, and ERTag is derived from the C-terminal transmembrane sequence from UBE2J2. (B) Diagram of the SpLacZ-MERCS reporter concept. The LacZ fragments are targeted separately to the surfaces of the mitochondria and ER. At regions where mitochondria and ER form contact sites (bottom panel), the split LacZ fragments are brought close enough to allow reconstitution of a functional protein, which is tetrameric. Nonfluorescent β-Gal substrate is then hydrolyzed into fluorescent or colorimetric products. (C) Phase contrast images of cells containing 6 pairs of split LacZ fragments after incubation with X-Gal. Images were taken with a 10× objective. (D) Quantification of (C). Particle analysis in ImageJ was used to measure the fraction of cells that were X-Gal positive. Data are shown as mean ± s.d. 20,000 cells were analyzed for each LacZ pair, in three independent experiments. *$p \leq 0.0001$. Statistical analysis was performed with the Student's t-test. U2OS cells were used. Scale bar = 200 μm. See also Figure S1.

have been engineered to directly visualize the contact sites.[18,19] However, reconstituted fluorescent proteins form thermodynamically stable complexes,[20] and in principle, the long half-life for dissociation may perturb normal MERCS dynamics or cause artificial tethering of membranes. Double-dimerizing green fluorescent protein (ddGFP) has been used in a MERCS reporter[21] but the signal-to-noise ratio is usually low in such systems. Fluorescence resonance energy transfer (FRET) and bioluminescence resonance energy transfer (BRET) have also been used to construct organellar contact sensors.[16] Because FRET/BRET methods do not require physical contact between the sensor partners, they avoid the potential problem of artificial tethering. However, these are proximity-based strategies and do not ensure that the signal arises from true physical contacts.[22]

All these reporters were designed to measure contacts sites at a specific point in time. However, MERCS are dynamic structures that assemble and disassemble depending on the physiological setting, and several cellular activities—organelle motility, organelle shaping, cell cycle—either regulate or depend on the dynamic nature of MERCS. A single time point measurement may not be an accurate representation of the overall MERCS content of a specific cell. As an example, mitochondrial fusion and fission events, which are regulated by MERCS, show stereotypical fluctuations as cells progress

https://doi.org/10.1021/acssynbio.4c00098
ACS Synth. Biol. 2024, 13, 2791−2803

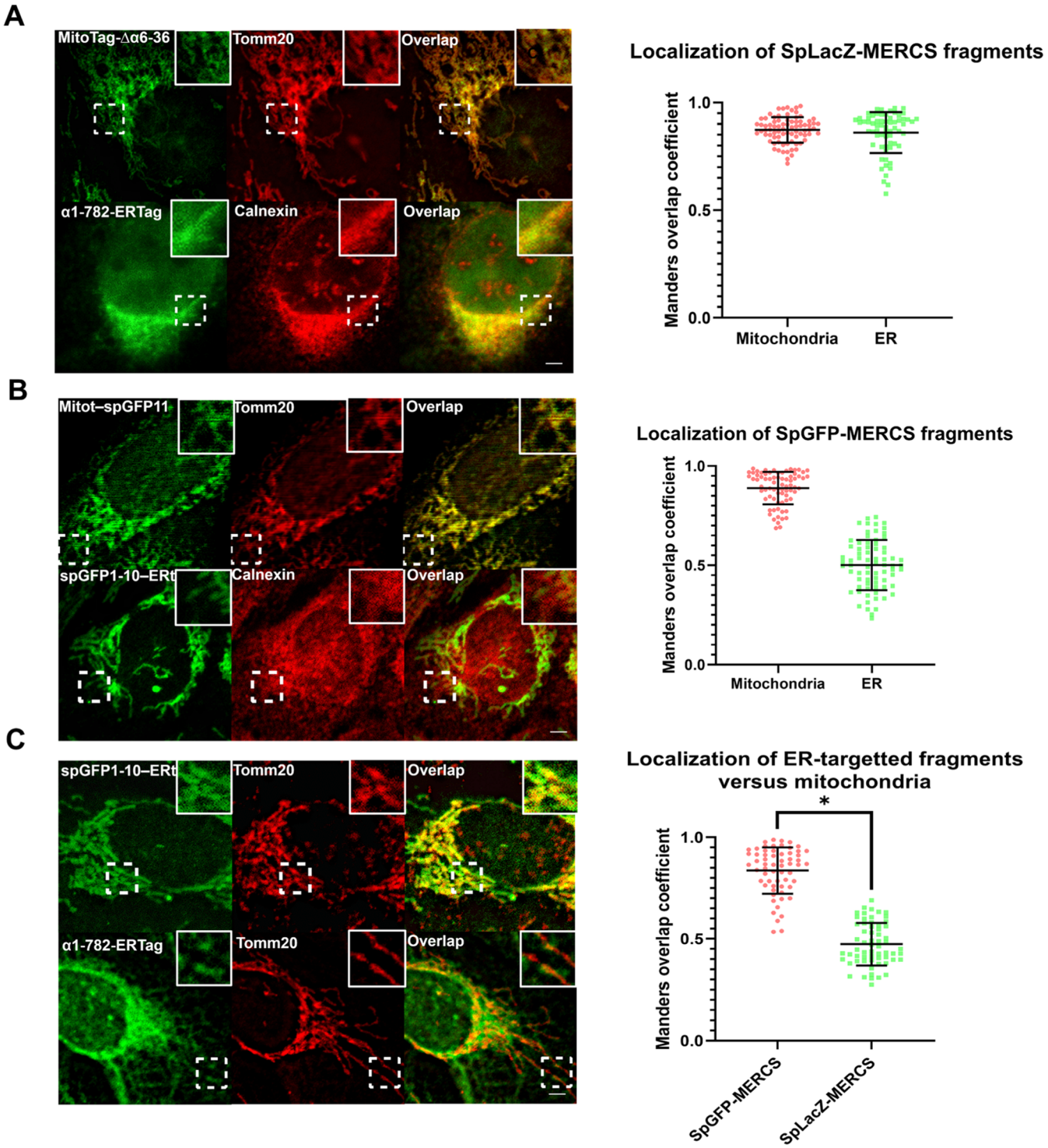

Figure 2. Comparison of the organellar targeting of SpLacZ-MERCS and SpGFP-MERCS fragments. Each panel show representative images on the left and the corresponding Manders coefficient analysis on the right. For the latter, three independent experiments were performed, and the mean ± s.d. for the combined data set is shown. (A) Targeting of SpLacZ-MERCS fragments in cells expressing both components of SpLacZ-MERCS. MitoTag-Δα6-36 (stained with anti-LacZ) was compared with the mitochondrial marker Tomm20, and α1-782-ERTag (stained with anti-V5) was compared with the ER marker Calnexin. 79 cells were analyzed for MitoTag-Δα6-36 and 65 cells for α1-782-ERTag. (B) Targeting of SpGFP-MERCS fragments in cells expressing both components of SpGFP-MERCS. MitoTag−SpGFP11 was compared with the mitochondrial marker Tomm20, and SpGFP1-10−ERTag was compared with the ER marker Calnexin. 74 cells were analyzed for MitoTag−SpGFP11 and 72 cells for SpGFP1-10−ERTag. (C) Comparison of the subcellular localizations of ER fragments from SpGFP-MERCS and SpLacZ-MERCS with the mitochondrial marker protein Tomm20. Both fragments were stained via the V5 protein tag. 61 cells were analyzed for SpGFP1-10−ERTag and 61 cells for α1-782-ERTag. *$p \leq 0.0001$. Statistical analysis was performed with the Student's t-test. U2OS cells were used. Scale bar = 2.5 μm. See also Figure S2.

through the cell cycle.[23] Moreover, the essentially irreversible nature of GFP complementation raises the concern that BiFC-based reporters do not faithfully respond to dynamic changes in the MERCS content. It would therefore be advantageous to have

https://doi.org/10.1021/acssynbio.4c00098
ACS Synth. Biol. 2024, 13, 2791−2803

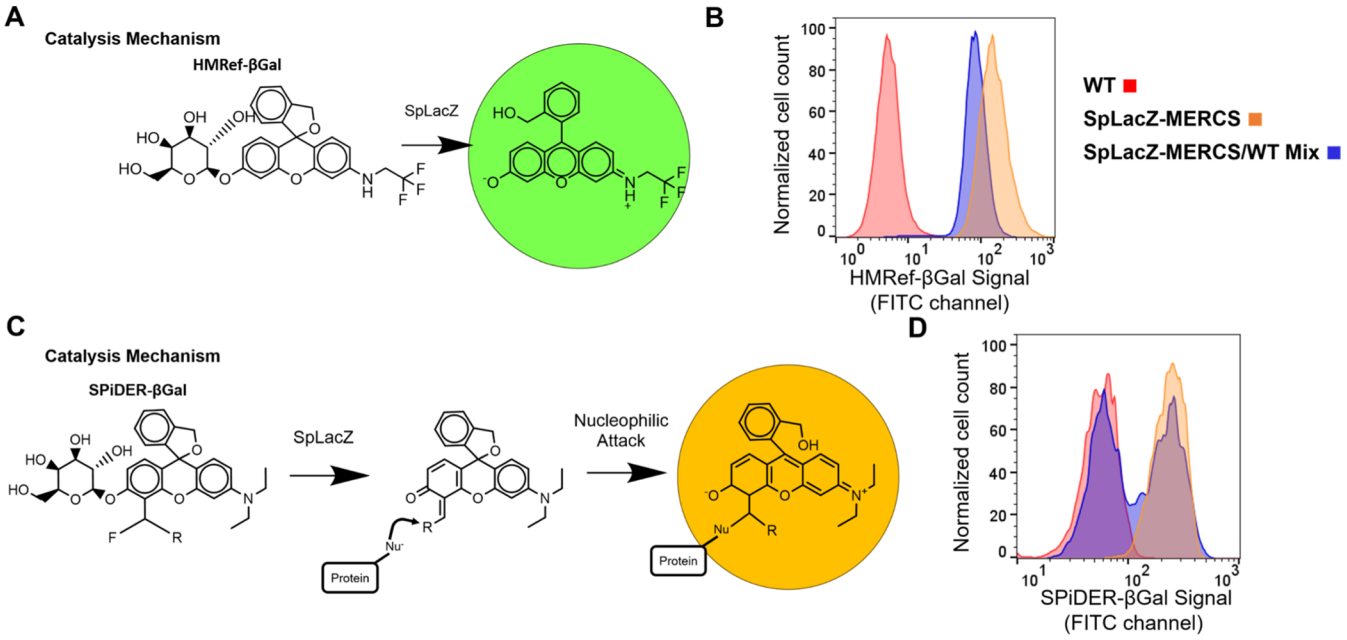

Figure 3. Comparison of β-galactosidase substrates for flow cytometry analysis of mixed cell populations. (A) Reaction mechanism for conversion of HMRef-βGal substrate into a soluble fluorescent product. The diagram is modified from Asanuma et al.[33] (B) Flow cytometry assay to determine cell autonomy of the fluorescence signal. After incubation of U2OS-WT and U2OS-SpLacZ-MERCS cells with HMRef-βGal (1 μM, 4 h), the two cell populations were mixed (blue) and compared by flow cytometry to the original control and U2OS-SpLacZ-MERCS cells. The mixed population shows a single peak located between the control and U2OS-SpLacZ-MERCS cells. (C) Reaction mechanism for conversion of Spider-βGal substrate into a reactive fluorescent product that covalently bonds with surrounding cellular proteins. The diagram is modified from Doura et al.[34] (D) Flow cytometry assay to determine cell autonomy of fluorescence signal. After incubation with Spider-βGal (0.25 μM, 4 h), a mixed population (blue) was compared to control and U2OS-SpLacZ-MERCS cells. The mixed population shows two separate peaks, one aligned with control cells and one aligned with U2OS-SpLacZ-MERCS cells. At least 25,000 cells were analyzed in each group per experiment. Three independent experiments were performed, and representative plots are shown. U2OS cells were used. See also Figure S3.

a MERCS reporter with integrative properties so that cells with overall high or low MERCS content can be accurately distinguished. Here, we designed the first MERCS reporter system with a fluorescent output that integrates information about the MERCS level over time. This reporter, termed SpLacZ-MERCS, utilizes α acceptor and α donor LacZ fragments targeted to the mitochondria and ER, respectively. The reporter accurately reads out the overall MERCS level and is responsive to dynamic fluctuations in mitochondria−ER interactions. We validated the ability of SpLacZ-MERCS to detect pharmacological and genetic perturbations known to affect MERCS. This reporter provides a new opportunity to investigate MERCS in high-throughput settings, including genome-wide gene perturbations and drug screening assays.

RESULTS AND DISCUSSION

Identification of Optimal LacZ Fragments for MERCS Reporter. In designing a new reporter to measure MERCS, we took advantage of the ability of weakly interacting fragments of β-galactosidase to reconstitute enzymatic activity. The bacterial LacZ gene, which encodes the enzyme β-galactosidase, exhibits α complementation, in which β-galactosidase containing an N-terminal truncation (termed α acceptor) can be complemented by an N-terminal peptide (termed α donor or α peptide) provided *in trans*.[24] Previous reports have described using α complementation with weakly interacting pairs of α donors and α acceptors to monitor protein−protein interactions in mammalian cells while avoiding artifactual physical interactions,[25−27] a concern with split GFP approaches due to the high stability of the reconstituted GFP. To adapt this system to study mitochondria−ER interactions in cultured cells, we started with a version of LacZ optimized for expression in mammalian cells.[28] Two types of α acceptors (LacZ $\Delta\alpha$ 6-36, LacZ $\Delta\alpha$ 6-78) were targeted to the mitochondrial outer membrane by fusion with the TOMM70 targeting sequence, and three types of α donor (LacZ α 1-75; LacZ α 1-141; and LacZ α 1-782) were targeted to the ER membrane by fusion with the UBE2J2 targeting sequence. Glycine-serine linkers were included to provide polypeptide chain flexibility for refolding and enzymatic complementation (Figure 1A). Figure 1B illustrates the premise that these membrane-anchored split-LacZ fragments can form a complex and reconstitute β-galactosidase enzymatic activity by α complementation only when the membranes of the mitochondria and ER in close proximity. Due to the weak interaction of LacZ fragments, the protein complex could dissociate when a contact site disassembles.

With two mitochondria-targeted α acceptors and three ER-targeted α donors, six different pairwise combinations were tested in U2OS cells. In previous studies, these LacZ fragment pairs were shown to have low affinity for each other, and enzyme activity was reconstituted only when the protein fragments were fused to other proteins that physically interact.[23] Both the MitoTag-$\Delta\alpha$6-36/α1-782-ERTag and $\Delta\alpha$6-78-MitoTag/α1-782-ERTag pairs showed substantial complementation, as evidenced by X-Gal staining (Figures 1C,D and S1A). The MitoTag-$\Delta\alpha$6-36/α1-782-ERTag pair showed the highest reconstituted activity and was used for further studies. Control cell lines expressing only individual LacZ fragments showed no ability to hydrolyze β-gal substrate (Figure S1B).

https://doi.org/10.1021/acssynbio.4c00098
ACS Synth. Biol. 2024, 13, 2791−2803

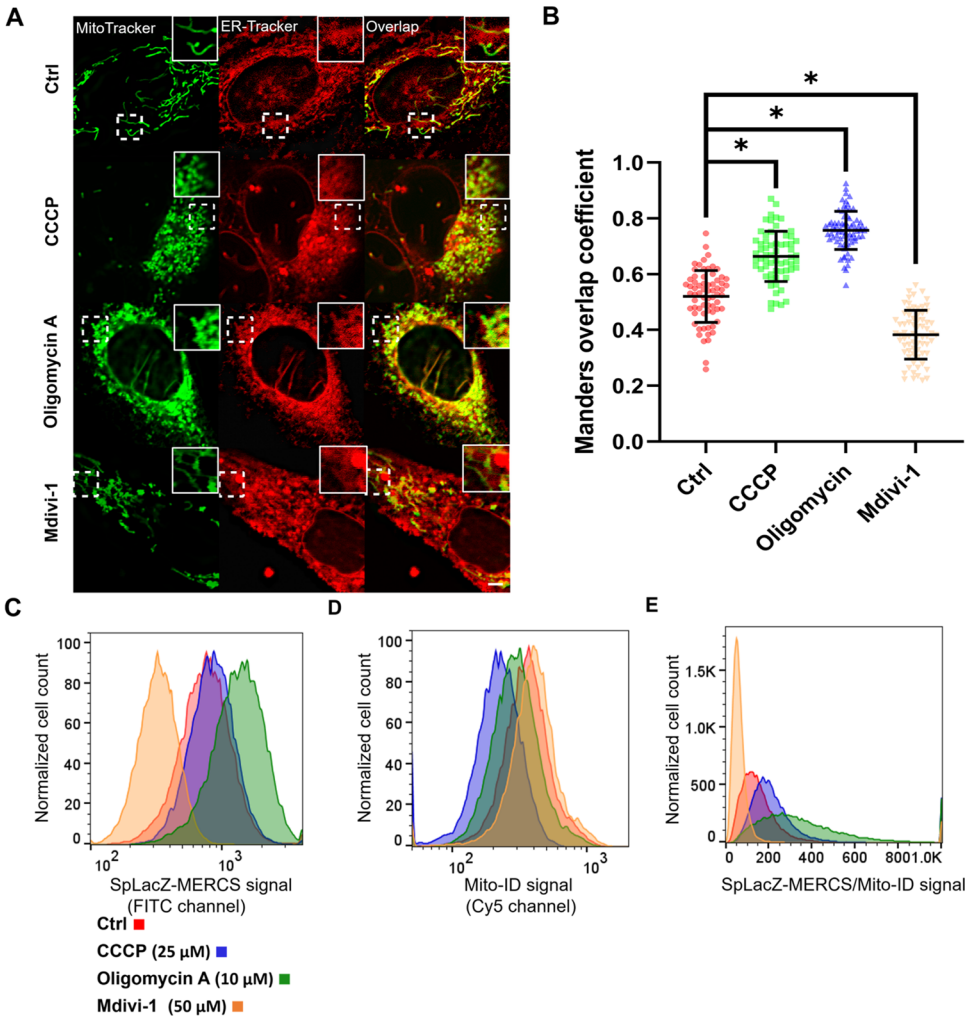

Figure 4. Effect of mitochondrial drugs on SpLacZ-MERCS signal. (A) Effect of mitochondrial drugs on colocalization of mitochondria and ER. The U2OS-SpLacZ-MERCS cell line was treated CCCP (25 μM, 4 h), oligomycin A (10 μM, 4 h), Mdivi-1 (50 μM, 4 h), or vehicle. Mitochondria and ER were analyzed by staining with MitoTracker and ER-Tracker. (B) Quantification of ER/mitochondrial colocalization under CCCP treatment, oligomycin A treatment, Mdivi-1 treatment, and nontreatment conditions. Manders overlap coefficient analysis is explained in the Methods section. Three independent experiments were performed, and mean ± s.d. for the combined data is shown $^*p \leq 0.0001$. In total, 68 cells were analyzed for the control; 63 cells were analyzed for CCCP; 75 cells were analyzed for oligomycin A; 71 cells were analyzed for Mdivi-1. (C) Effect of selected drugs on the SpLacZ-MERCS signal. Flow cytometry was used to quantify the SpLacZ-MERCS reporter signal (0.25 μM Spider-βGal, 4 h). (D) Effect of mitochondrial drugs on the Mito-ID signal. Mito-ID stains mitochondria regardless of membrane potential and can be used as a proxy for mitochondrial mass. Flow cytometry was used to quantify the Mito-ID signal. (E) Effect of mitochondrial drugs on the SpLacZ-MERCS signal after correction for mitochondrial mass. Cells were incubated with Spider-βGal and Mito-ID and analyzed by flow cytometry. The plot shows the Spider-βGal/Mito-ID ratio on the x-axis. For (C)−(E), a representative experiment from three independent experiments is shown. At least 25,000 cells were analyzed in each group per experiment. U2OS cells were used. Scale bar = 2.5 μm. See also Figure S4.

Using immunofluorescence on cells coexpressing LacZ MitoTag-Δα6-36 and LacZ α1-782-ERTag, we confirmed that LacZ MitoTag-Δα6-36 colocalized with the mitochondrial marker Tomm20, and LacZ α1-782-ERTag colocalized with the ER marker Calnexin (Figure 2A). We similarly evaluated the previously established split-GFP-based MERCS reporter system (referred to as SpGFP-MERCS hereafter), which uses the same TOMM70 and UBE2J2 targeting sequences to target GFP11 to mitochondria (Mitot−spGFP11) and GFP1-10 to the ER (spGFP1-10−ERt).[19] In cells coexpressing Mitot−spGFP11 and spGFP1-10−ERt, the mitochondrially targeted fragment colocalized with Tomm20. However, the spGFP1-10−ERt fragment appeared in tubular structures that did not colocalize with Calnexin (Figure 2B). Instead, the spGFP1-10−ERt-positive tubules colocalized with Tomm20 (Figure 2C). The corresponding LacZ α1-782-ERTag fragment did not show this organellar mislocalization (Figure 2C). The mislocalization did not occur when spGFP1-10−ERt was expressed in the absence of MitoTag−SpGFP11 (Figure S2A), indicating that mislocalization was likely induced by the high binding affinity between GFP11 and GFP1−10.[20,29]

Because expression of artificial tethers can increase mitochondria−ER contact,[30−32] we tested whether the expression of the SpLacZ-MERCS reporter perturbed normal mitochondria−ER interactions. We performed immunofluorescence against Tomm20 and Calnexin, and used confocal microscopy to assess the degree of overlap between the mitochondrial and ER signals. To benchmark this method, we also imaged the same signals with the Zeiss Airyscan in super-resolution mode. Using the Manders coefficient analysis to measure the fraction of ER signal colocalizing with mitochondrial signal, we found that standard confocal microscopy and

https://doi.org/10.1021/acssynbio.4c00098
ACS Synth. Biol. 2024, 13, 2791−2803

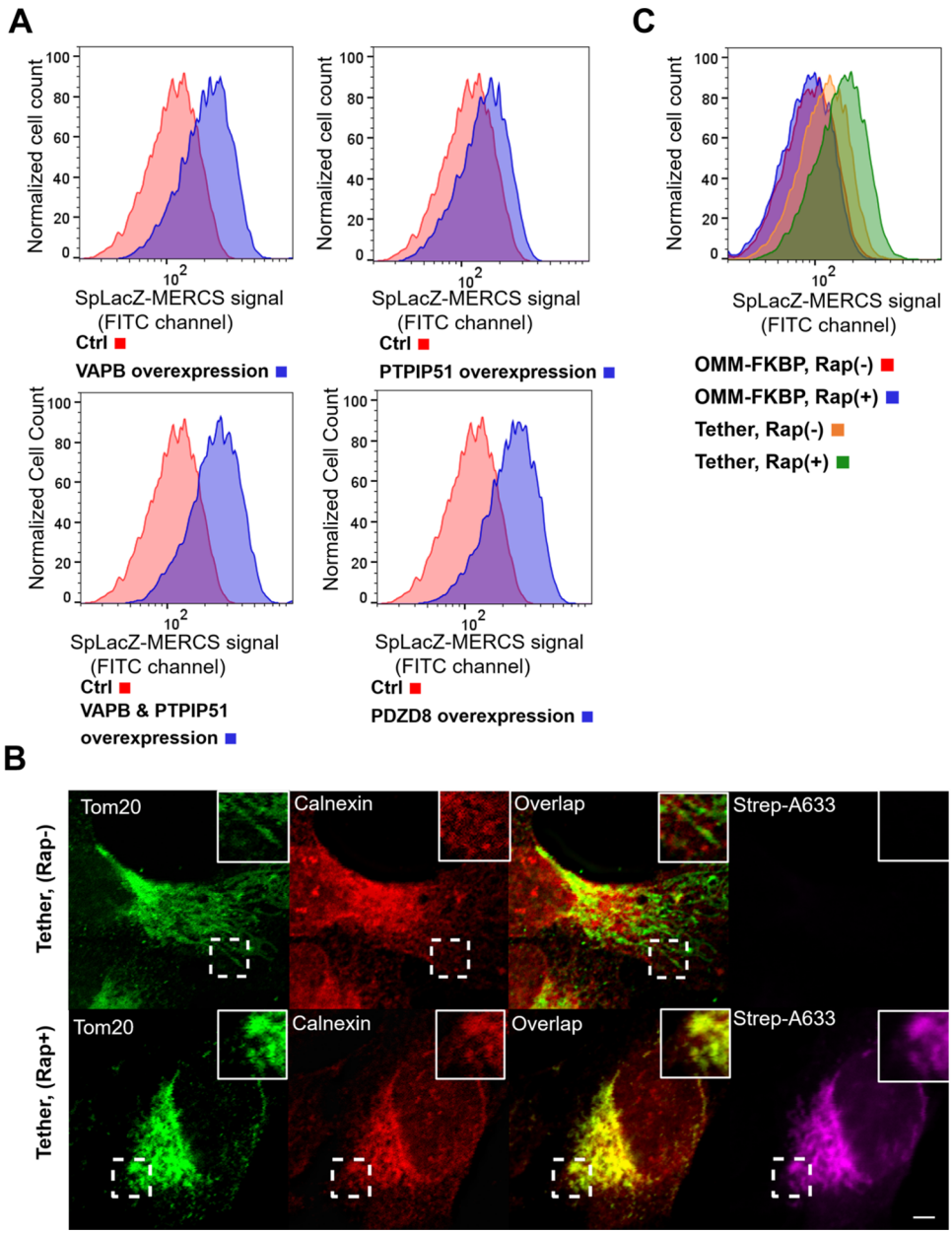

Figure 5. Effect of native and artificial tethers on the SpLacZ-MERCS signal. (A) Effect of overexpressed native tethers on the SpLacZ-MERCS signal. Flow cytometry was used to quantify the SpLacZ-MERCS signal (0.25 μM Spider-βGal, 4 h) upon stable expression of VAPB, PTPIP51, both VAPB and PTPIP51, and PDZD8. (B) Effect of artificial tether on mitochondria/ER colocalization. Cells expressed the SpTurboID FKBP-FRB system (tether). Upon rapalog (Rap) addition (bottom panel), mitochondria and ER are artificially tethered. ER and mitochondria colocalization were analyzed by immunofluorescence against Calnexin and Tomm20, respectively. Rapalog treatment also reconstitutes biotinylation activity,[37] which was detected by staining with streptavidin-Alexa Fluor 633. (C) Effect of artificial tethering on the SpLacZ-MERCS signal. Flow cytometry was used to quantify the SpLacZ-MERCS reporter signal (0.25 μM Spider-βGal, 4 h) in cells expressing the SpTurboID FKBP-FRB system (Tether) or only one component as a control (OMM-FKBP). Rapalog addition was used to mediate tethering in the former. In (A) and (C), a representative experiment from three independent experiments is shown. At least 25,000 cells were analyzed in each group per experiment. U2OS cells were used. Scale bar = 2.5 μm. See also Figure S5.

super-resolution microscopy gave similar results. In particular, both methods showed similar enhancement of mitochondria−ER overlap with overexpression of the VAPB/PTPIP51 tethers or an artificial tether (Figure S2B), and similar reduction of mitochondria−ER overlap with knockdown of the PDZD8 or VAPB tethers (Figure S2C). Due to the similar performance of both imaging methods, the rest of this study shows results using standard confocal microscopy. Importantly, we found that cells expressing the SpLacZ-MERCS reporter showed no change in the levels of colocalization between the mitochondria and ER (Figure S2D).

Spider-βGal Substrate Enables Single-cell MERCS Measurement. HMRef-βGal is a LacZ substrate that produces green fluorescence in live cells upon hydrolysis by β-galactosidase (structure and catalysis mechanism shown in Figure 3A).[33] After incubation with HMRef-βGal, cells expressing SpLacZ-MERCS showed increased fluorescence compared to wild-type control cells. However, when a 1:1 mixture of the control cells and SpLacZ-MERCS-expressing

https://doi.org/10.1021/acssynbio.4c00098
ACS Synth. Biol. 2024, 13, 2791−2803

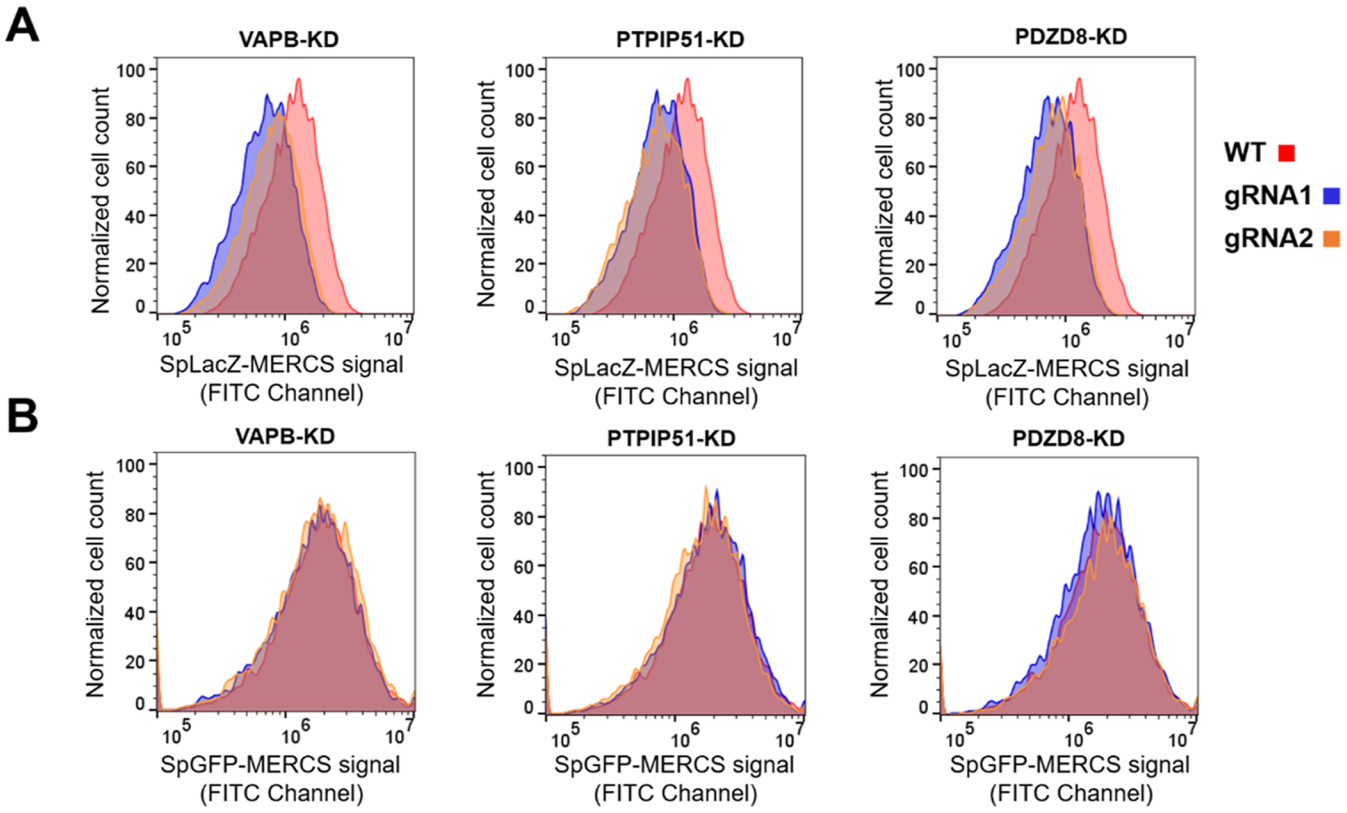

Figure 6. Effect of disruption of endogenous tethers on the SpLacZ-MERCS signal. (A) Effects of VAPB, PTPIP51, and PDZD8 knockdowns on the SpLacZ-MERCS signal. Flow cytometry was used to quantify the SpLacZ-MERCS signal (0.25 μM Spider-βGal, 4 h). (B) Effects of tether knockdowns on the SpGFP-MERCS reporter signal. Flow cytometry was used to quantify the SpGFP-MERCS signal. In (A) and (B), a representative experiment from three independent experiments is shown. At least 12,000 cells are analyzed in each group per experiment. U2OS cells were used. See also Figure S6.

cells was analyzed, only a single, intermediate peak appeared on flow cytometry (Figure 3B). The presence of the intermediate peak suggests that the fluorescent product leaks out of SpLacZ-MERCS-expressing cells and is taken up by control cells. This cell retention problem indicates that the HMRef-βGal substrate is not suitable for measuring the MERCS level in individual cells within a population.

To circumvent this problem, we tested Spider-βGal, an alternative β-galactosidase substrate whose cleavage product is a reactive quinone methide intermediate that reacts with cellular proteins and therefore does not leak out of the cell.[34] Figure 3C shows the mechanism of action and structure of Spider-βGal. We confirmed that the SpLacZ-MERCS-expressing cells, in contrast to cells expressing a single SpLacZ fragment, converted Spider-βGal to its fluorescent state (Figure S3A). Importantly, when we mixed an equal number of control cells with SpLacZ-MERCS cells, two distinct peaks were found that corresponded to the positive and negative cell populations on flow cytometry (Figure 3D). These results suggest that Spider-βGal has no cell leakage and can be used for fluorescence-based analysis of SpLacZ-MERCS. We have also confirmed that most of the Spider-βGal fluorescent signal is retained hours after removal of the substrate (Figure S3B).

The SpLacZ-MERCS Reporter Detects Drug-induced MERCS Defects. To test whether SpLacZ-MERCS can detect differences in MERCS levels caused by drugs, we examined the effect of oligomycin A, CCCP, and Mdivi-1 on mitochondria−ER colocalization and the SpLacZ-MERCS signal. Oligomycin A is an ATP synthase inhibitor that causes mitochondrial fission, a process that involves wrapping of the ER around mitochondrial tubules to cause constriction.[35] CCCP (carbonyl cyanide *m*-chlorophenyl hydrazone) disrupts the mitochondrial membrane potential and also induces mitochondria fission. Mdivi-1 (Mitochondrial division inhibitor 1) is an inhibitor of DRP1 with off-target effects on Complex I.[36,37] As expected, oligomycin A and CCCP treatment resulted in substantial mitochondrial fragmentation associated with an increase in mitochondria−ER contacts, as measured by MitoTracker/ER-Tracker colocalization. In contrast, Mdivi-1 treatment resulted in a hyperfused mitochondria network with reduced mitochondria−ER colocalization (Figure 4A,B).

The SpLacZ-MERCS signal was dramatically increased by oligomycin A, moderately increased by CCCP, and decreased by Mdivi-1 (Figure 4C). CCCP is known to induce mitophagy and reduce mitochondrial content.[38] To normalize for mitochondrial content, we stained mitochondria with Mito-ID, a dye that marks mitochondria irrespective of membrane potential. There was a substantial reduction in Mito-ID staining after CCCP treatment (Figure 4D). Upon normalization for mitochondrial content, both CCCP and oligomycin A treatment caused substantial increases in the SpLacZ-MERCS signal, whereas Mdivi-1 caused a decrease (Figure 4E). Control experiments showed that these drugs did not interfere with the β-galactosidase hydrolysis reaction (Figure S4A). In contrast to SpLacZ-MERCS, the SpGFP-MERCS signal was static, failing to show a response to any of the drug treatments (Figure S4B). We also found that the Spider-βGal incubation time or the Spider-βGal substrate level could be optimized to improve the

https://doi.org/10.1021/acssynbio.4c00098
ACS Synth. Biol. 2024, 13, 2791−2803

signal-to-noise separation (Figure S4C,D). Moreover, the SpLacZ-MERCS reporter was capable of distinguishing increasing levels of MERCS perturbation caused by increasing concentrations of oligomycin A (Figure S4E).

SpLacZ-MERCS Signal is Increased by Overexpression of Native and Artificial Mitochondria−ER Tethers. We tested whether our reporter responded to overexpression of native mitochondria−ER tethers. Three of the most well-characterized mitochondria−ER tethers are VAPB, PTPIP51, and PDZD8. VAPB and PTPIP51 are interacting proteins that localize to the ER and mitochondria, respectively, and are known to facilitate calcium transfer, lipid transfer, and regulation of mitochondria quality control.[10,11,13,15] PDZD8 is an integral ER membrane protein that has also been found to be important for mitochondria−ER contacts.[12] Overexpression of either VAPB, PTIPIP51, or PDZD8 increased the activity of the SpLacZ-MERCS reporter. Cells overexpressing both VAPB and PTPIP51 showed an even greater increase in the SpLacZ-MERCS signal (Figures 5A and S5A).

We then investigated the effect of artificial tethering of mitochondria−ER membranes on the SpLacZ-MERCS signal. The split-TurboID FKBP-FRB system[39] is an artificial tether in which one component (SpTurbo(N)-OMM-FKBP) is localized to the mitochondrial outer membrane, and the other component (SpTurbo(C)-ER-FRB) is localized to the ER membrane. Strong association of the two membranes is triggered by rapalog, a small molecule that mediates binding between FKBP and FRB (Figure S5B). Rapalog also results in the reconstitution of TurboID, an engineered biotin ligase.[39] Upon addition of rapalog to cells expressing the SpTurbo-FKBP-FRB system and SpLacZ-MERCS, we observed an increase in mitochondria−ER colocalization, biotinylation activity, and the SpLacZ-MERCS signal (Figure 5B,C).

SpLacZ-MERCS Signal is Reduced by the Knockdown of MERCS Tethers. We investigated the effect of knocking down native mitochondria−ER tethering factors. Using CRISPRi, we performed knockdowns of VAPB, PTPIP51 and PDZD8 in cells expressing either SpLacZ-MERCS or SpGFP-MERCS. For each tethering protein, successful knockdown for two gRNAs was confirmed by Western blotting (Figure S6A). Knockdown of VAPB, PTPIP51, or PDZD8 all resulted in lower SpLacZ-MERCS signal by flow cytometry (Figure 6A). However, the same knockdowns did not affect the SpGFP-MERCS signal (Figure 6B). For each of these knockdowns, mitochondrial mass, as measured by Mito-ID analysis, was not affected (Figure S6B). To further test whether SpLacZ-MERCS can detect different degrees of MERCS disruption, we performed a more quantitative analysis of the VAPB, PTPIP51, and PDZD8 knockdown experiments. Based on quantification of Western blots, gRNA1 is reproducibly more effective than gRNA2 for VAPB knockdown (Figure S6C). The knockdown efficiencies for gRNA1 and gRNA2 were indistinguishable for PTPIP51 and PDZD8. These data on knockdown efficiency correlate well with flow cytometry analysis of the SpLacZ-MERCS reporter. In particular, gRNA1 for VAPB shows a stronger suppression of the SpLacZ-MERCS signal (Figure S6D).

SpLacZ-MERCS can Detect MERCS Defects caused by Disease Genes. We tested whether the MERCS reporter is capable of detecting MERCS defects implicated in neurodegenerative disease, especially amyotrophic lateral sclerosis (ALS).[40,41] Overexpression of the RNA/DNA binding protein TDP-43 and its ALS-related mutants results in disruption of MERCS.[42,43] SIGMAR1 is another protein associated with ALS,[44] and its knockdown disrupts mitochondrial-ER calcium homeostasis.[45] Upon overexpressing TDP-43 or the mutant TDP-43 (G348C), we observed notable decreases in the SpLacZ-MERCS signal, with a stronger effect for the mutant (Figures 7A and S7A,B). The knockdown of SIGMAR1 also resulted in a lower SpLacZ-MERCS signal (Figures 7B and S7C).

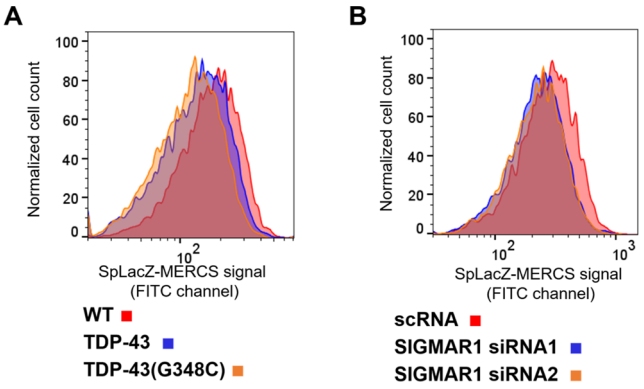

Figure 7. Effect of disease-related genes on the SpLacZ-MERCS signal. (A) Effect of TDP-43 (WT) and TDP-43 (G348C) overexpression on the SpLacZ-MERCS signal. (B) Effect of SIGMAR1 knockdown on the SpLacZ-MERCS signal. In (A) and (B), U2OS cells were incubated with 0.25 μM Spider-βGal for 4 h, and flow cytometry was used to quantify the SpLacZ-MERCS signal. A representative experiment from three independent experiments is shown. At least 12,000 cells were analyzed for each sample per experiment. See also Figure S7.

SpLacZ-MERCS can Accurately Track MERCS Dynamics. To test the ability of SpLacZ-MERCS to monitor MERCS dynamics, we performed time-lapse confocal imaging to evaluate the dynamics of the SpLacZ-MERCS signal against that of ER-mitochondria colocalization. Early stage images of SpLacZ-MERCS show puncta formation at the interface between mitochondria and ER (Figure 8A). The puncta become progressively larger and diffuse over time (Supporting Information File S2). In time-lapse analysis, individual cells show temporal fluctuations in mitochondria−ER colocalization that correlated well with the dynamics of the SpLacZ-MERCS signal (Figure 8B,D). Upon treatment of cells with oligomycin A to induce mitochondrial fission, cells showed a progressive increase in mitochondria−ER colocalization that correlated well with the increase in the SpLacZ-MERCS signal (Figure 8C,D). Under both conditions, the dynamics of the SpLacZ-MERCS signal and mitochondria/ER colocalization were highly correlated (Figure 8D). The range of the SpLacZ-MERCS signal dynamics has a magnitude similar to that of the mitochondria−ER colocalization under both conditions (Figure 8E,F). Thus, our data suggests that SpLacZ-MERCS is capable of accurately capturing MERCS dynamics.

CONCLUSIONS

MERCS are dynamic interorganellar interfaces that coordinate the activities of the ER and mitochondria, including calcium homeostasis, lipid biosynthesis, mitochondrial dynamics, and mitochondrial quality control. Considering the importance of this topic, it is critical to have an accurate MERCS reporter that overcomes the limitations of current systems. In this study, we developed a MERCS reporter system that generates a

https://doi.org/10.1021/acssynbio.4c00098
ACS Synth. Biol. 2024, 13, 2791−2803

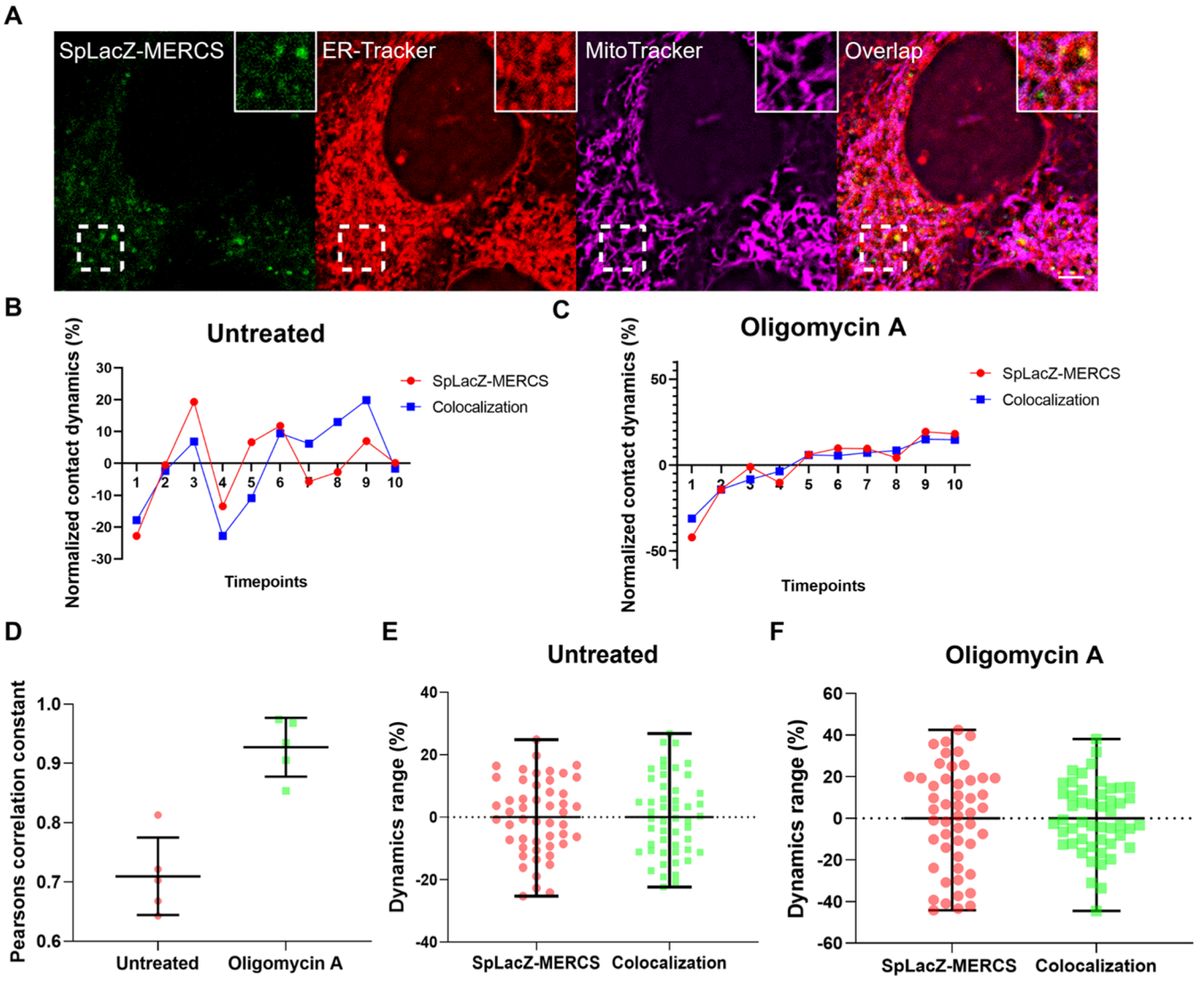

Figure 8. Tracking of MERCS dynamics by SpLacZ-MERCS reporter. (A) Representative single frames from a time-lapse movie of cells harboring the SpLacZ-MERCS reporter and treated with Spider-βGal (0.25 μM). (B) Comparison of contact dynamics measured by the SpLacZ-MERCS reporter versus mitochondria/ER colocalization in untreated cells. For the SpLacZ-MERCS reporter, "normalized contacts dynamics" is calculated at each time point as the difference in fluorescence intensity between the last and the current time point, normalized to the mean fluorescence value (eqs 1 and 3). For mitochondria−ER colocalization, "normalized contacts dynamics" at each time point is the average of the Manders coefficient for mitochondria−ER colocalization for the last and current time point, normalized to the mean value (eqs 2 and 4). Negative values indicate decreasing MERCS levels; zero indicates unchanged MERCS levels; positive values indicate increasing MERCS levels. The plots indicate the temporal fluctuations in MERCS dynamics occurring during normal culture. (C) Comparison of contacts dynamics measured by the SpLacZ-MERCS reporter versus mitochondria/ER colocalization, after oligomycin A addition. Note that both measurements show progressive increases in MERCS content with time. (D) Correlation of the dynamics of the SpLacZ-MERCS signal to that of mitochondria/ER colocalization. Pearson correlation constants are shown for untreated cells and cells treated with oligomycin A. Data are shown as mean ± s.d. for 5 cells. (E) The ranges of the contact dynamics measured by SpLacZ-MERCS and mitochondria/ER colocalization in untreated cells. (F) The ranges of the contact dynamics measured by SpLacZ-MERCS and mitochondria/ER colocalization after oligomycin A addition. For (E) and (F), three independent experiments were performed to yield 50 data points, and the mean ± s.d. is shown. U2OS cells were used. Scale bar = 2.5 μm.

fluorescent signal that accumulates over time and, therefore, integrates the cellular history of the MERCS signal. SpLacZ-MERCS combined with the Spider-βGal substrate enables the accurate analysis of MERCS levels within individual cells of a population. We identified a LacZ α acceptor and α donor pair that functions well together when targeted to mitochondria and ER respectively. Each reporter fragment was cleanly trafficked to its respective compartment. Although correct organellar targeting may seem trivial, we found that the ER component of the SpGFP-MERCS reporter has a high degree of mislocalization to mitochondria when expressed by our retroviral expression system. This mislocalization is likely caused by the essentially irreversible binding of split-GFP fragments.

The SpLacZ-MERCS reporter responded well to drug and genetic manipulations that affect the interaction between the mitochondria and ER. The drugs CCCP, oligomycin A, and Mdivi-1 all affected mitochondria−ER colocalization and have a corresponding effect on the SpLacZ-MERCS signal. Overexpression of the well-characterized tethers VAPB, PTPIP51, and PDZD8 each resulted in an increase in the SpLacZ-MERCS signal. Expression of an artificial FKBP/FRB-based mitochondria−ER tethering system also resulted in a significant increase

https://doi.org/10.1021/acssynbio.4c00098
ACS Synth. Biol. 2024, 13, 2791−2803

in SpLacZ-MERCS signal upon chemically induced dimerization. Knockdowns of VAPB, PTPIP51, or PDZD8 reduced the SpLacZ-MERCS signal. In contrast, the SpGFP-MERCS reporter failed to respond to the knockdown of known tethers. Disease-related MERC defects can also be identified through SpLacZ-MERCS. Time-lapse studies showed that the SpLacZ-MERCS reporter is able to track dynamic fluctuations in the MERCS level.

The integrative signal produced from the SpLacZ-MERCS reporter is advantageous in evaluating individual cells for their overall MERCS levels. Mitochondria−ER interactions are dynamic, and cells are expected to have fluctuations in their MERCS level due to factors such as organelle motility, organelle shaping, and cell cycle. These fluctuations complicate the ability of other MERCS reporters to score cells as having high or low levels of MERCS, whereas SpLacZ-MERCS can accurately reflect the overall MERCS level. This system enables new opportunities for the high-throughput screening of genes or drugs that regulate MERCS levels. A caveat is that our MERCS reporter cumulatively records the MERCS level over time, which prevents the visualization of exact contact sites. Our methodology may be applicable to studying the crosstalk of other organelles, like mitochondria-peroxisome and mitochondria−lysosome interactions.

METHODS

Antibodies and Reagents. *Primary Antibodies.* TOMM20 (Santa Cruz BioTech, sc-17764), CALX (Proteintech, 66903-1-Ig), MYC (Sigma, C3956), FLAG M2 (Sigma, F1804-200UG), HA.11 (Covance, MMS-101R), PDZD8 (Proteintech, 25512-1-AP), VAPB (Proteintech, 14477-1-AP), PTPIP51 (Proteintech, 20641-1-AP).

Secondary Antibodies. Goat antimouse IgG (H + L)-HRP (Jackson ImmunoResearch, 115-035-003), goat antirabbit IgG (H + L)-HRP (Jackson ImmunoResearch, 111-035-003), donkey antimouse IgG AlexaFluor 405 (abcam, ab175658), donkey antimouse IgG AlexaFluor 488 (Invitrogen, A21202), donkey antirabbit IgG AlexaFluor 555 (Invitrogen, A32794), goat antirabbit IgG AlexaFluor 633 (Invitrogen, A21070).

Chemicals. Carbonyl cyanide 3-chlorophenylhydrazone (CCCP) (Sigma-Aldrich, C2759), Mdivi-1 (Sigma-Aldrich, M0199), oligomycin A (Sigma-Aldrich, O4876), Spider-βGal (Dojindo, SG02), rapalog (Takara Bio, 635056), BioTracker 519 Green β-Gal Dye (Millipore Sigma, SCT025).

siRNAs. SIGMAR1 siRNA 1: hs.Ri.SIGMAR1.13.1 (IDT); SIGMAR1 siRNA 2: hs.Ri.SIGMAR1.13.2 (IDT), scrambled negative control DsiRNA: 51-01-19-09 (IDT).

Plasmid Construction. Primer sequences are listed in Supporting Information File S3. For the construction of LacZ donors plasmids, LacZ α1-75, α1-147, and α1-782 were amplified using the common forward primer Comdon-F and the reverse primers S-R, M-R, and L-R. The ER targeting sequence was amplified from plx304-spGFP1−10-Ert[19] with primers ER-F and ER-R. NotI/MfeI-digested LacZ donor fragment and MfeI/BamHI-digested ERTAG were ligated with NotI/BamHI-digested backbone (PQCXIP-mCherry retroviral vector).

For the construction of LacZ acceptors plasmids, LacZ $\Delta\alpha$6-36, and $\Delta\alpha$6-78 were amplified respectively using the forward primers 1-F and 2-F, and a common reverse primer Comrec-R. The mito targeting sequence was amplified from pLVX -Mitot-spGFP11 × 2[19] with primers Mito_F and Mito_R. The NotI/MfeI-digested LacZ acceptor fragment and MfeI/NotI-digested MitoTag were ligated with NotI/BamHI-digested backbone (PQCXIP-PURO retroviral vector).

For the construction of VAPB, PTPIP51, and VAPB/PTPIP51 expressing plasmids, the pUltra (Addgene Plasmid #24129) lentiviral vector is used as the backbone. The marker was modified from GFP to hygromycin by amplifying the hygromycin resistance gene with HYG_F and HYG_R and ligating into AgeI/BsrGI-digested pUltra. VAPB was amplified with VA_F and VA_R; PTPIP51 was amplified with PTP_F and PTP_R. VAPB and PTPIP51 ORFs were inserted into pUltra_Hyg. For the construction of PDZD8 expressing plasmid, PDZD8−3XHA was amplified from pCAG-PDZD8HA with PDZ_F and PDZ_R and inserted into PQCXIP-Neo digested with NotI/AgeI.

The gRNA plasmids were constructed by inserting annealed oligos into the lentiviral CRISPRia-v2 backbone (Addgene, 84832) at the BstXI/BlpI sites. For two gRNAs targeting VAPB, the following oligonucleotides were annealed: YP.190 and YP.191; YP.192 and YP.193. For the two gRNAs targeting PTPIP51, the following oligonucleotides were annealed: YP.196 and YP.197; YP.198 and YP.199. For the two gRNAs targeting PDZD8, the following oligonucleotides were annealed: YP.202 and YP.203; YP.204 and YP.205. The gRNA control had the following protospacer sequence: gctcggtcccgcgtcgtcgg.

The TDP43 overexpression plasmid was constructed by amplifying the TDP43-ORF with primers TDP43-1 and TDP43-2, and Gibson assembled onto pUltra-mCherry based on NheI/EcoRI digestion sites. The TDP43(G348C) overexpression plasmid was constructed by amplifying the TDP43-ORF with primers TDP43-1/3 and TDP43-2/4 and Gibson assembled onto pUltra-mCherry based on NheI/EcoRI digestion sites.

Cell Culture and Generation of Stable Cell Lines. U2OS and HEK293T cells were grown in Dulbecco's modified Eagle medium (DMEM) supplemented with 10% fetal bovine serum (FBS), 2 mM glutamine, and 1% penicillin-streptomycin, at 37 °C with 5% CO_2. To produce retrovirus, HEK293T cells were transfected by the calcium phosphate method with packaging plasmids (pVSV-G and pUMVC) and retroviral constructs. For lentivirus production, HEK293T cells were transfected with pVSV-G, pΔ8.9, and lentiviral constructs. Fresh media was added 12 h after transfection. 48 h after transfection, the supernatant was collected and passed through a 0.45 μm syringe filter to remove cell debris. HeLa cells or K562 cells were transduced in the presence of 8 μg/mL Polybrene (Sigma, H9268). To select for transduced cells, puromycin (1 μg/mL) or hygromycin (80 μg/mL) was applied for at least 3 days or 7 days, respectively.

Flow Cytometry. Flow cytometry analysis was performed with the S3e Cell Sorter (488/561 nm). For experiments knocking down endogenous MERCS tethers, BFP positive cells were sorted on a CytoFLEX S (Beckman Coulter).

To prepare for flow cytometry, cells were trypsinized, neutralized with Fluorobrite complete medium, and spun down at 300*g* for 8 min. Cells are washed once with ice-cold Fluorobrite complete medium and resuspended in Fluorobrite complete medium containing 20 mM 4-(2-hydroxyethyl)-1-piperazineethanesulfonic acid (HEPES) before analysis and sorting. All flow cytometry data were analyzed in FlowJo v10.8 Software (BD Life Sciences).

Immunostaining and Live Cell Imaging. For immunofluorescence imaging, cells were fixed in 4% paraformaldehyde in phosphate-buffered saline (PBS), washed three times with PBS,

https://doi.org/10.1021/acssynbio.4c00098
ACS Synth. Biol. 2024, 13, 2791−2803

and permeabilized with 0.1% Triton X-100 for 30 min. Cells were washed three times with PBS and blocked in PBS containing 10% FBS for 30 min. Fixed cells were further incubated overnight in the cold room with primary antibodies. Cells were washed with PBS three times and incubated with secondary antibodies at room temperature for 1 h and washed four times with PBS before imaging.

For measurements of mitochondria−ER colocalization, cells were washed and incubated with complete DMEM medium containing 200 nM MitoTracker Deep Red FM and 500 nM ER-Tracker Blue-White DPX for 30 min at 37 °C. Cells were washed three times and incubated in complete Flourbrite medium containing 10% fetal bovine serum, 2 mM glutamine, and penicillin-streptomycin before live cell imaging.

For both Immunofluorescence imaging and live cell imaging, images were obtained with a Zeiss LSM 710 confocal microscope (Carl Zeiss). Images were analyzed using ImageJ.

Manders Overlap Coefficient Analysis. For Figure 2A, the Manders overlap coefficients measure the fraction of Tomm20 signal that overlapped with MitoTag-Δα6-36 signal, and the fraction Calnexin signal that overlapped with α1-782-ERTag signal. For Figure 2B, the Manders overlap coefficients measure the fraction of Tomm20 signal that overlapped with Mitot−spGFP11 signal, and the fraction of Calnexin signal that overlapped with spGFP1-10−ERt signal. For Figure 2C, the Manders overlap coefficients measure the fraction of Tomm20 signal that overlapped with spGFP1-10−ERt signal, and the fraction of Tomm20 signal that overlapped with α1-782-ERTag signal. For Figures 4 and 8, the Manders overlap coefficients measure the fraction of ER-Tracker signal that overlapped with MitoTracker signal. For Figure S2A, the Manders overlap coefficients measured the fraction of Calnexin signal that overlapped with spGFP1-10−ERt signal. For Figure S2B−D, the Manders overlap coefficients measured the fraction of Calnexin signal that overlapped with the Tomm20 signal.

Drug Treatments. The following drug concentrations were used: CCCP, 10 μM; Mdivi-1, 50 μM; oligomycin A1, 10 μg/mL. Cells were incubated with these drugs for 4 h before flow cytometry or live-cell imaging.

Analysis of SpLacZ-MERCS Dynamics. To analyze the dynamics of the SpLacZ-MERCS signal, 11 images from a time-series were used for each cell. $F_{\mathrm{SpLacZ}}(n)$ is defined as cell fluorescence level at time point n measured by SpLacZ-MERCS. $D_{\mathrm{SpLacZ}}(n)$ is the change in contact dynamics based on the SpLacZ-MERCS reporter signal at data point n. $\mu_{D_{\mathrm{SpLacZ}}}$ is defined as the mean value of the 10 D_{SpLacZ} data points. $\widehat{D_{SpLacZ}(n)}$ is defined as D_{SpLacZ} at time point n normalized to the mean D_{SpLacZ} value.

$M(n)$ is defined as the Manders overlap coefficient between mitochondria and ER at time point n. $D_{\mathrm{Overlap}}(n)$ is the change in contact dynamics calculated based on mitochondria/ER colocalization at data point n. $\mu_{D_{\mathrm{Overlap}}}$ is defined as the mean value of the 10 D_{Overlap} data points. $\widehat{D_{Overlap}(n)}$ is defined as D_{Overlap} at time point n normalized to the mean D_{Overlap} value.

$$D_{\mathrm{SpLacZ}}(n) = F_{\mathrm{SpLacZ}}(n+1) - F_{\mathrm{SpLacZ}}(n) \quad (n = 1, 2, 3, \ldots, 10) \tag{1}$$

$$D_{\mathrm{Overlap}}(n) = \frac{M(n+1) + M(n)}{2} \quad (n = 1, 2, 3, \ldots, 10) \tag{2}$$

$$\widehat{D_{\mathrm{SpLacZ}}(n)} = \frac{D_{\mathrm{SpLacZ}}(n) - \mu_{D_{\mathrm{SpLacZ}}}}{\mu_{D_{\mathrm{SpLacZ}}}} \times 100\% \quad (n = 1, 2, 3, \ldots, 10)\ldots \tag{3}$$

$$\widehat{D_{\mathrm{overlap}}(n)} = \frac{D_{\mathrm{overlap}}(n) - \mu_{D_{\mathrm{overlap}}}}{\mu_{D_{\mathrm{overlap}}}} \times 100\% \ (n = 1, 2, 3, \ldots, 10) \tag{4}$$

Rapalog-induced Mitochondria−ER Tethering. The constructs pLX208 CMV sTurboID (C)-HA-FRB-ERM (Addgene plasmid #153007) and pLX304 CMV OMM-FKBP-V5-sTurboID (N) (Addgene plasmid #153006) were used to induce artificial tethering between mitochondria and ER. Cells were incubated with 500 nM rapalog and 50 μM of biotin for 24 h for immunofluorescence imaging. For flow cytometry, cells were incubated with only rapalog.

Statistical Analysis. The statistical analysis was performed using GraphPad Prism 9. All data were shown as mean ± standard deviation; raw data are provided in Supporting Information File S4. Statistical analysis among different groups was performed with the Student's *t*-test.

■ ASSOCIATED CONTENT

Supporting Information

The Supporting Information is available free of charge at https://pubs.acs.org/doi/10.1021/acssynbio.4c00098.

Details on the behavior of LacZ fragment pairs (Figure S1); comparison of SpGFP-MERCS and SpLacZ-MERCS subcellular localization and a comparison of mitochondria−ER overlap measurements (Figure S2); SpLacZ-MERCS fluorescence (Figure S3); effect of mitochondrial drugs on the SpLacZ-MERCS signal (Figure S4); expression of natural and artificial mitochondria−ER tethers (Figure S5); knockdown of endogenous mitochondria−ER tethers (Figure S6), and disease gene expression or knockdown (Figure S7) (PDF)

A time-lapse movie of Spider-βGal fluorescence (MP4)

List of DNA primers used in this study (XLSX)

Raw data, included data points and uncropped Western blots (XLSX)

■ AUTHOR INFORMATION

Corresponding Author

David C. Chan − *Division of Biology and Biological Engineering, California Institute of Technology, Pasadena, California 91125, United States;* orcid.org/0000-0002-0191-2154; Email: dchan@caltech.edu

Author

Zheng Yang − *Division of Biology and Biological Engineering, California Institute of Technology, Pasadena, California 91125, United States*

Complete contact information is available at: https://pubs.acs.org/10.1021/acssynbio.4c00098

Author Contributions

Z.Y. and D.C.C. formulated the research plan, and Z.Y. performed the experiments. Z.Y. and D.C.C. wrote the manuscript.

Funding

This work was supported by NIH grant R35GM127147.

Notes

The authors declare no competing financial interest.

■ ACKNOWLEDGMENTS

We thank the members of the Chan laboratory for helpful comments on the manuscript.

■ ABBREVIATIONS

ATP:adenosine triphosphate
BRET:bioluminescence resonance energy transfer
CCCP:carbonyl cyanide *m*-chlorophenyl hydrazone
ER:endoplasmic reticulum
FRET:fluorescence resonance energy transfer
GFP:green fluorescent protein
MERCS:mitochondria−endoplasmic−reticulum contact sites

■ REFERENCES

(1) Martínez-Reyes, I.; Chandel, N. S. Mitochondrial TCA Cycle Metabolites Control Physiology and Disease. *Nat. Commun.* **2020**, *11* (1), No. 102, DOI: 10.1038/s41467-019-13668-3.
(2) Spinelli, J. B.; Haigis, M. C. The Multifaceted Contributions of Mitochondria to Cellular Metabolism. *Nat. Cell Biol.* **2018**, *20* (7), 745−754.
(3) Suen, D. F.; Norris, K. L.; Youle, R. J. Mitochondrial Dynamics and Apoptosis. *Genes Dev.* **2008**, *22* (12), 1577−1590.
(4) Lezi, E.; Swerdlow, R. H. Mitochondria in Neurodegeneration. *Adv. Exp. Med. Biol.* **2012**, *942*, 269−286.
(5) Harrington, J. S.; Ryter, S. W.; Plataki, M.; Price, D. R.; Choi, A. M. K. Mitochondria in Health, Disease, and Aging. *Physiol. Rev.* **2023**, *103* (4), 2349−2422.
(6) Gordaliza-Alaguero, I.; Cantó, C.; Zorzano, A. Metabolic Implications of Organelle−Mitochondria Communication. *EMBO Rep.* **2019**, *20* (9), No. e47928, DOI: 10.15252/embr.201947928.
(7) Marchi, S.; Patergnani, S.; Pinton, P. The Endoplasmic Reticulum-Mitochondria Connection: One Touch, Multiple Functions. *Biochim. Biophys. Acta, Bioenerg.* **2014**, *1837* (4), 461−469.
(8) Phillips, M. J.; Voeltz, G. K. Structure and Function of ER Membrane Contact Sites with Other Organelles. *Nat. Rev. Mol. Cell Biol.* **2016**, *17* (2), 69−82.
(9) Giacomello, M.; Pellegrini, L. The Coming of Age of the Mitochondria−ER Contact: A Matter of Thickness. *Cell Death Differ.* **2016**, *23* (9), 1417.
(10) Gomez-Suaga, P.; Paillusson, S.; Stoica, R.; Noble, W.; Hanger, D. P.; Miller, C. C. J. The ER-Mitochondria Tethering Complex VAPB-PTPIP51 Regulates Autophagy. *Curr. Biol.* **2017**, *27* (3), 371.
(11) Gómez-Suaga, P.; Pérez-Nievas, B. G.; Glennon, E. B.; Lau, D. H. W.; Paillusson, S.; Mórotz, G. M.; Calì, T.; Pizzo, P.; Noble, W.; Miller, C. C. J. The VAPB-PTPIP51 Endoplasmic Reticulum-Mitochondria Tethering Proteins Are Present in Neuronal Synapses and Regulate Synaptic Activity. *Acta Neuropathol. Commun.* **2019**, *7* (1), No. 35, DOI: 10.1186/s40478-019-0688-4.
(12) Hirabayashi, Y.; Kwon, S. K.; Paek, H.; Pernice, W. M.; Paul, M. A.; Lee, J.; Erfani, P.; Raczkowski, A.; Petrey, D. S.; Pon, L. A.; Polleux, F. ER-Mitochondria Tethering by PDZD8 Regulates Ca2+ Dynamics in Mammalian Neurons. *Science* **2017**, *358* (6363), 623−630.
(13) Stoica, R.; Vos, K. J.; Paillusson, S.; Mueller, S.; Sancho, R. M.; Lau, K. F.; Vizcay-Barrena, G.; Lin, W. L.; Xu, Y. F.; Lewis, J.; Dickson, D. W.; Petrucelli, L.; Mitchell, J. C.; Shaw, C. E.; Miller, C. C. J. ER−Mitochondria Associations Are Regulated by the VAPB−PTPIP51 Interaction and Are Disrupted by ALS/FTD-Associated TDP-43. *Nat. Commun.* **2014**, *5* (1), No. 3996.
(14) Aoyama-Ishiwatari, S.; Hirabayashi, Y. Endoplasmic Reticulum−Mitochondria Contact Sites—Emerging Intracellular Signaling Hubs. *Front. Cell Dev. Biol.* **2021**, *9*, No. 653828.
(15) De Vos, K. J.; Mórotz, G. M.; Stoica, R.; Tudor, E. L.; Lau, K.-F.; Ackerley, S.; Warley, A.; Shaw, C. E.; Miller, C. C. J. VAPB Interacts with the Mitochondrial Protein PTPIP51 to Regulate Calcium Homeostasis. *Hum. Mol. Genet.* **2012**, *21* (6), 1299−1311.
(16) Giamogante, F.; Barazzuol, L.; Brini, M.; Calì, T. ER−Mitochondria Contact Sites Reporters: Strengths and Weaknesses of the Available Approaches. *Int. J. Mol. Sci.* **2020**, *21* (21), 1−18.
(17) Wilson, E. L.; Metzakopian, E. ER-Mitochondria Contact Sites in Neurodegeneration: Genetic Screening Approaches to Investigate Novel Disease Mechanisms. *Cell Death Differ.* **2021**, *28* (6), 1804−1821.
(18) Shai, N.; Yifrach, E.; Roermund, C. W. T.; Cohen, N.; Bibi, C.; Ijlst, L.; Cavellini, L.; Meurisse, J.; Schuster, R.; Zada, L.; Mari, M. C.; Reggiori, F. M.; Hughes, A. L.; Escobar-Henriques, M.; Cohen, M. M.; Waterham, H. R.; Wanders, R. J. A.; Schuldiner, M.; Zalckvar, E. Systematic Mapping of Contact Sites Reveals Tethers and a Function for the Peroxisome-Mitochondria Contact. *Nat. Commun.* **2018**, *9* (1), No. 1761.
(19) Yang, Z.; Zhao, X.; Xu, J.; Shang, W.; Tong, C. A Novel Fluorescent Reporter Detects Plastic Remodeling of Mitochondria-ER Contact Sites. *J. Cell Sci.* **2018**, *131*, 1.
(20) Romei, M. G.; Boxer, S. G. Split Green Fluorescent Proteins: Scope, Limitations, and Outlook. *Annu. Rev. Biophys.* **2019**, *48*, 19.
(21) Abrisch, R. G.; Gumbin, S. C.; Wisniewski, B. T.; Lackner, L. L.; Voeltz, G. K. Fission and Fusion Machineries Converge at ER Contact Sites to Regulate Mitochondrial Morphology. *J. Cell Biol.* **2020**, *219*, No. e201911122.
(22) Hertlein, V.; Flores-Romero, H.; Das, K. K.; Fischer, S.; Heunemann, M.; Calleja-Felipe, M.; Knafo, S.; Hipp, K.; Harter, K.; Fitzgerald, J. C.; García-Sáez, A. J. MERLIN: A Novel BRET-Based Proximity Biosensor for Studying Mitochondria−ER Contact Sites. *Life Sci. Alliance* **2020**, *3* (1), No. e201900600, DOI: 10.26508/LSA.201900600.
(23) Mitra, K.; Wunder, C.; Roysam, B.; Lin, G.; Lippincott-Schwartz, J. A Hyperfused Mitochondrial State Achieved at G1-S Regulates Cyclin E Buildup and Entry into S Phase. *Proc. Natl. Acad. Sci. U.S.A.* **2009**, *106* (29), 11960−11965.
(24) Jacob, F.; Monod, J. Genetic Regulatory Mechanisms in the Synthesis of Proteins. *J. Mol. Biol.* **1961**, *3* (3), 318−356.
(25) Mohler, W. A.; Blau, H. M. Gene Expression and Cell Fusion Analyzed by LacZ Complementation in Mammalian Cells. *Proc. Natl. Acad. Sci. U.S.A.* **1996**, *93* (22), 12423−12427.
(26) Rossi, F.; Charlton, C. A.; Blau, H. M. Monitoring Protein-Protein Interactions in Intact Eukaryotic Cells by Beta-Galactosidase Complementation. *Proc. Natl. Acad. Sci. U.S.A.* **1997**, *94* (16), 8405−8410.
(27) Thormeyer, D.; Ammerpohl, O.; Larsson, O.; Xu, Y.; Asinger, A.; Wahlestedt, C.; Liang, Z. Characterization of LacZ Complementation Deletions Using Membrane Receptor Dimerization. *Biotechniques* **2003**, *34* (2), 346−355.
(28) Wu, S.; Ying, G.; Wu, Q.; Capecchi, M. R. A Protocol for Constructing Gene Targeting Vectors: Generating Knockout Mice for the Cadherin Family and Beyond. *Nat. Protoc.* **2008**, *3* (6), 1056−1076.
(29) Liu, T. Y.; Chou, W. C.; Chen, W. Y.; Chu, C. Y.; Dai, C. Y.; Wu, P. Y. Detection of Membrane Protein−Protein Interaction in Planta Based on Dual-Intein-Coupled Tripartite Split-GFP Association. *Plant J.* **2018**, *94* (3), 426−438.
(30) Csordás, G.; Renken, C.; Várnai, P.; Walter, L.; Weaver, D.; Buttle, K. F.; Balla, T.; Mannella, C. A.; Hajnóczky, G. Structural and Functional Features and Significance of the Physical Linkage between ER and Mitochondria. *J. Cell Biol.* **2006**, *174* (7), 915−921.
(31) Kornmann, B.; Currie, E.; Collins, S. R.; Schuldiner, M.; Nunnari, J.; Weissman, J. S.; Walter, P. An ER-Mitochondria Tethering Complex Revealed by a Synthetic Biology Screen. *Science* **2009**, *325* (5939), 477.
(32) Shi, F.; Kawano, F.; Park, S. E.; Komazaki, S.; Hirabayashi, Y.; Polleux, F.; Yazawa, M. Optogenetic Control of Endoplasmic

Reticulum−Mitochondria Tethering. *ACS Synth. Biol.* **2018**, *7* (1), 2−9.
(33) Asanuma, D.; Sakabe, M.; Kamiya, M.; Yamamoto, K.; Hiratake, J.; Ogawa, M.; Kosaka, N.; Choyke, P. L.; Nagano, T.; Kobayashi, H.; Urano, Y. Sensitive β-Galactosidase-Targeting Fluorescence Probe for Visualizing Small Peritoneal Metastatic Tumours in Vivo. *Nat. Commun.* **2015**, *6* (1), No. 6463.
(34) Doura, T.; Kamiya, M.; Obata, F.; Yamaguchi, Y.; Hiyama, T. Y.; Matsuda, T.; Fukamizu, A.; Noda, M.; Miura, M.; Urano, Y. Detection of LacZ-Positive Cells in Living Tissue with Single-Cell Resolution. *Angew. Chem., Int. Ed.* **2016**, *55* (33), 9620−9624.
(35) Friedman, J. R.; Lackner, L. L.; West, M.; DiBenedetto, J. R.; Nunnari, J.; Voeltz, G. K. ER Tubules Mark Sites of Mitochondrial Division. *Science* **2011**, *334* (6054), 358−362.
(36) Bordt, E. A.; Clerc, P.; Roelofs, B. A.; Saladino, A. J.; Tretter, L.; Adam-Vizi, V.; Cherok, E.; Khalil, A.; Yadava, N.; Ge, S. X.; Francis, T. C.; Kennedy, N. W.; Picton, L. K.; Kumar, T.; Uppuluri, S.; Miller, A. M.; Itoh, K.; Karbowski, M.; Sesaki, H.; Hill, R. B.; Polster, B. M. The Putative Drp1 Inhibitor Mdivi-1 Is a Reversible Mitochondrial Complex I Inhibitor That Modulates Reactive Oxygen Species. *Dev. Cell* **2017**, *40* (6), 583−594.e6.
(37) Cassidy-Stone, A.; Chipuk, J. E.; Ingerman, E.; Song, C.; Yoo, C.; Kuwana, T.; Kurth, M. J.; Shaw, J. T.; Hinshaw, J. E.; Green, D. R.; Nunnari, J. Chemical Inhibition of the Mitochondrial Division Dynamin Reveals Its Role in Bax/Bak-Dependent Mitochondrial Outer Membrane Permeabilization. *Dev. Cell* **2008**, *14* (2), 193−204.
(38) Mauro-Lizcano, M.; Esteban-Martínez, L.; Seco, E.; Serrano-Puebla, A.; Garcia-Ledo, L.; Figueiredo-Pereira, C.; Vieira, H. L. A.; Boya, P. New Method to Assess Mitophagy Flux by Flow Cytometry. *Autophagy* **2015**, *11* (5), 833.
(39) Cho, K. F.; Branon, T. C.; Rajeev, S.; Svinkina, T.; Udeshi, N. D.; Thoudam, T.; Kwak, C.; Rhee, H. W.; Lee, I. K.; Carr, S. A.; Ting, A. Y. Split-TurboID Enables Contact-Dependent Proximity Labeling in Cells. *Proc. Natl. Acad. Sci. U.S.A.* **2020**, *117* (22), 12143−12154.
(40) Hartopp, N.; Markovinovic, A.; Miller, C. C.; Gomez-Suaga, P. Insight into Endoplasmic Reticulum-Mitochondria Contacts in Human Amyotrophic Lateral Sclerosis. *Neural Regener. Res.* **2024**, *19* (7), 1407.
(41) Chen, J.; Bassot, A.; Giuliani, F.; Simmen, T. Amyotrophic Lateral Sclerosis (ALS): Stressed by Dysfunctional Mitochondria-Endoplasmic Reticulum Contacts (MERCs). *Cells* **2021**, *10* (7), No. 1789.
(42) Stoica, R.; De Vos, K. J.; Paillusson, S.; Mueller, S.; Sancho, R. M.; Lau, K.-F.; Vizcay-Barrena, G.; Lin, W.-L.; Xu, Y.-F.; Lewis, J.; Dickson, D. W.; Petrucelli, L.; Mitchell, J. C.; Shaw, C. E.; Miller, C. C. J. ER−Mitochondria Associations Are Regulated by the VAPB−PTPIP51 Interaction and Are Disrupted by ALS/FTD-Associated TDP-43. *Nat. Commun.* **2014**, *5*, No. 3996.
(43) Tamaki, Y.; Urushitani, M. Molecular Dissection of TDP-43 as a Leading Cause of ALS/FTLD. *Int. J. Mol. Sci.* **2022**, *23* (20), No. 12508.
(44) Herrando-Grabulosa, M.; Gaja-Capdevila, N.; Vela, J. M.; Navarro, X. Sigma 1 Receptor as a Therapeutic Target for Amyotrophic Lateral Sclerosis. *Br. J. Pharmacol.* **2021**, *178* (6), 1336−1352.
(45) Tagashira, H.; Bhuiyan, M. S.; Shinoda, Y.; Kawahata, I.; Numata, T.; Fukunaga, K. Sigma-1 Receptor Is Involved in Modification of ER-Mitochondria Proximity and Ca2+ Homeostasis in Cardiomyocytes. *J. Pharmacol. Sci.* **2023**, *151* (2), 128−133.

https://doi.org/10.1021/acssynbio.4c00098
ACS Synth. Biol. 2024, 13, 2791−2803